Highly conductive and transparent aluminum-doped zinc oxide thin films deposited on polyethylene terephthalate substrates by pulsed laser deposition

L. M. Wong[a], S. Y. Chiam[a], W. K. Chim[b], J. S. Pan[a], S. J. Wang [a,1]

[a] Institute of Materials Research and Engineering, A*STAR (Agency for Science, Technology and Research), 3 Research Link, Singapore 117602, Singapore,

[b] Department of Electrical and Computer Engineering, National University of Singapore, 4 Engineering Drive 3, Singapore 117576, Singapore

[1] Fax: (65) 6872-0785; Tel: (65) 6874-8184; Email: sj-wang@imre.a-star.edu.sg

Abstract

High transparent conductive aluminum-doped zinc oxide thin films were deposited on low-cost flexible polyethylene terephthalate substrates at room temperature using pulsed laser deposition and the effects of oxygen pressure and film thickness on film properties were investigated. It was found that grain sizes play only a greater role at smaller film thicknesses in affecting the carrier mobility. Resistivity changes at larger film thickness can be caused by near surface/interface depletion that affected both mobility and carrier concentration. The inherent film transparency did not change and any reduction in the film transmittance is likely related to a thickness dependent attenuation effect. This means that different transparent conducting oxides should each possess an optimum film thickness, whereby optimized zinc oxide is typically about 100 nm. A low resistivity of ~6.6×10^{-4} Ω-cm with a high normalized transparency index of >0.9 for a 110 ± 10 nm thick room-temperature deposited film was obtained, representing one of the best results obtained to date.

Keywords: transparent conducting oxide, aluminum zinc oxide, pulsed laser deposition, polyethylene terephthalate, thickness dependence, AZO, PLD, TCO

1. Introduction

Transparent conducting oxides (TCOs) deposited on polymeric substrates are subjects of extensive research efforts to enable the development of electronic devices for applications in photovoltaics, displays, transistors and electrochromics on flexible substrates [1-5]. The TCOs generally have to exhibit a resistivity not exceeding the order of 10^{-3} Ω-cm and have an average transmittance of above 80% in the visible region to be considered suitable for application as a transparent electrode [6]. Indium tin oxide (ITO) is currently the most commonly used TCO in many applications of electronic and optical devices [7-11]. However, ITO is not only considered to be toxic and expensive, it typically requires a heat treatment of over 300 °C to achieve the desired high transparency and low resistivity, making it difficult for applications using polymer based materials [12-14]. Therefore, there is an urgent need to seek alternative materials that can effectively substitute the use of ITO at lower process temperature to advance the development of electronic or optical devices on plastic substrates [15-20]. A lower process temperature also allows for potential usage of TCOs as the top electrode in polymer based devices without possible device degradation due to heat treatment [1, 21]. Zinc oxide (ZnO), with a wide direct band gap of 3.34 eV, is one potential candidate that is non-toxic, abundant and inexpensive. ZnO exhibits high transparency in the visible region and can possibly be doped with group III elements such as aluminum or gallium to improve its electrical properties [22-24].

The development of applications on polymer substrates has many advantages. A typical glass substrate suffers from being brittle and excessively heavy. Development of transparent electrodes on flexible plastic substrates provides realistic solutions for a

flexible, lightweight, robust and cost-effective starting substrate that can be of great importance to portable, large area or niche devices [25-27].

In the design of a transparent electrode on polymer substrates using thin film technology, the film thickness of the TCO is of great importance since it is directly related to the strain that it can withstand. Hence, a thinner TCO results in greater flexibility since the critical radius of a thin film is proportional to the film thickness [28]. Unfortunately, it is generally reported that thinner TCOs results in films of lower conductivity [29]. Thus far, it is a challenge to produce thin oxide layers with suitably low resistivity. For example, the lowest resistivity reported for gallium-doped zinc oxide deposited on polyethylene terephthalate (PET) substrates at room temperature is ~7.8×10^{-4} Ω-cm but this is for a relatively thick 800 nm film [18]. However, for TCO in the range of about 100 nm, the lowest resistivity is reported by Gadre *et al*. with a value of ~ 4 x 10^{-3} Ω-cm for a 85 nm thick indium gallium zinc oxide film on polyethylene naphthalate substrates, and this is only achievable after a 150°C post-deposition anneal [30]. The nature of the dependence of resistivity, or even transparency, on film thickness is not widely reported and it is therefore important to conduct more investigations to understand the dependency. In this study, we deposited aluminum doped zinc oxide (AZO) thin films at room temperature on PET substrates using pulsed laser deposition (PLD) without any post-deposition annealing. We first examine the crystallographic structure, optical and electrical properties of these films as a function of oxygen pressure to optimize the deposited film properties. At the optimized growth condition, we varied the thickness of the deposited AZO film on PET substrates and discuss the effects on resistivity and transparency.

2. Experimental procedures

AZO thin films were deposited on 125 μm thick polymeric PET substrates using the PLD technique with a ZnO:Al (1.5 wt.% Al_2O_3) ceramic target of purity 99.999%. The PLD uses a KrF excimer laser (wavelength of 248 nm and 25 ns pulse width) operating at a repetition rate of 20 Hz with a total energy of 300 mJ. The deposition chamber was evacuated to a base pressure of 1.3 x 10^{-6} Pa. The target-substrate distance was maintained at 6 cm during the deposition while the oxygen pressure was varied from 2.6 x 10^{-3} to 1.3 Pa. The entire deposition process was performed at room temperature and typical thickness of the films was about 110 ± 10 nm. In the second part of the experiments, at a chosen oxygen pressure (which gives optimum results), we repeated the deposition process for different duration to achieve different film thicknesses. All the film thicknesses were measured using the Veeco multi-mode atomic force microscope (AFM) nanoscope IV Tapping Mode mode. Optical measurements were performed using a Shimadzu double beam UV-3600 UV-VIS-NIR spectrophotometer and electrical characterization was carried out using the HL5500PC Hall effect measurement system via the Van der Pauw method at room temperature using indium as contacts. Crystallinity of the films was measured using an X-ray-diffraction (XRD) system, equipped with Cu $K\alpha$ (λ = 1.5466Å) radiation with Graphite monochromator and a HI-STAR 2D General Area Detector. The 2-theta scan was done with the detector employed at 3 detection angles with a scanning of the Omega axis at each angle.

3. Results and discussion

3.1 Effect of oxygen pressure: Optical and electrical properties

A summary of the optical properties, together with the measured resistivity of AZO films deposited at room temperature, is shown in figure 1. The plot shows the measured resistivity and normalized transparency indices at different oxygen pressures. The resistivities of the films at the respective conditions are obtained from Hall effect measurements. The normalized transparency indices represent the fraction of transmission at various indicated spectral ranges after accounting for variations in film thickness. From our previous publication [31], the normalized index T_x is shown in equation (1) as follows:

$$T_x = \frac{\sum_{n=280}^{1700} \Gamma_n \times e^{-\alpha_n (x-d)} \times I_n}{\sum_{n=280}^{1700} I_n} \quad (1)$$

where Γ_n (%) is the measured transmittance at the wavelength n (nm), I_n is the intensity of the spectrum with a unit of $Wm^{-2}nm^{-1}$, x is an arbitrary choice of normalization film thickness suitable for the specific application (eg. x=110 nm), d is the actual thickness of the film in the transmittance measurement and α_n is the absorption coefficient at the particular wavelength. In this work, although our thicknesses do not vary greatly, we have used equation (1) to give a more accurate transparency index. We use a normalization thickness of 110 nm and obtain the absorption coefficient from the transmittance at different wavelengths [31]. Thickness normalization in this aspect is critical to understand the optical properties of the film itself. Different thicknesses give variations in transmittance and this should be corrected for in order to understand the film properties at each deposition condition. The use of the normalized index can also

be useful for applications in different devices and separation into different wavelength regions can help the understanding of film properties [31]. Figure 1 shows that for the visible wavelength range, an oxygen pressure of above 1.3×10^{-3} Pa will be sufficient to result in a film with transmittance of greater than 80%, with the transmittance saturating at higher oxygen pressure. The overall normalized transparency appears to gradually increase with oxygen pressure, with a high transmittance of ~90% at oxygen pressures of 1×10^{-2} Pa or larger. The corresponding resistivity, however, shows optimum values in the mid-oxygen pressure regime, with higher resistivities measured at both lower and higher oxygen pressures.

The XRD spectra for all the AZO films grown on PET substrates obtained under various oxygen pressures show a peak at 34.4°, which is consistent with the ZnO (002) diffraction peak (figure 2(a)). This shows that all the films have a polycrystalline hexagonal wurtzite structure that is highly oriented along the c-axis [32, 33]. Using the Scherrer's formula, we note that there are slight variations in the calculated grain sizes that range from (14.6 - 17.6) ± 1 nm for the various oxygen pressures. A plot of the mobility and overall resistivity for the different calculated grain sizes in figure 2(b) showed no clear trends. This shows that such small changes in grain sizes may not be significant in affecting the transport properties, and other scattering mechanism (besides grain size) is affecting the mobility.

The electrical property of the AZO film is shown in figure 3 where the mobility, carrier concentration and resistivity are plotted against the different oxygen pressure during deposition. The improvement in resistivity for lower oxygen partial pressure can

be observed to be due to the significant increase in carrier mobility. This can be due to a reduction in deep-level defects that can improve the carrier mobility by reducing scattering. This agrees with the concomitant improvements in transparency since a reduction of these defects will improve transmittance in the visible range and this is similarly observed in figure 1. This also means that, while defect scattering is dominant, grain boundary scattering may play a less significant role as was discussed. The increase in resistivity at higher oxygen partial pressures shown in figure 3 can be attributed to both a decrease in carrier concentration and mobility. The large decrease in carrier concentration should increase the infrared transmittance and our transparency index in the infrared range, shown in figure 1, agrees with this interpretation. The smaller increase, or similar overall transparency, can be explained by the accompanying reduction of transmittance in the ultra-violet region by variation of the band gap through the Burstein Moss effect. This competing factor can be shown by examination of our measured band gap variations. The band gap (E_g) of the AZO film on PET substrate is found through computing the absorption coefficient (α) from transmittance measurements using the Beer-Lambert's attenuation equation [34].The film thickness is measured using the AFM and the derived Tauc's plot is shown in figure 4. The optical E_g is obtained from a linear extrapolation in the plot of $(\alpha h\upsilon)^2$ and photon energy ($h\upsilon$), which yields an optical E_g ranging from ~3.49 to 3.7 eV. The Burstein-Moss shift generally describes a case whereby the lower energy interband transition is blocked and the measured optical band gap is enhanced, and the change in band gap is related to the electron concentration as: [35-37]

$$\Delta E_g = \frac{\hbar^2}{2m^*}\left(3\pi^2 n_e\right)^{2/3} \quad (1)$$

where ΔE_g denotes the optical bang gap shift, ħ is the reduced Planck constant, m^* is the reduced effective mass ($\frac{1}{m^*} = \frac{1}{m_v^*} + \frac{1}{m_c^*}$) and n_e is the carrier concentration. Figure 5 shows the plot of carrier concentration as a function of a change in the optical band gap according to Eq. (1), where we have used the optical band gap of 3.29 eV that is measured from our undoped ZnO film as the reference. The good linear relationship through the origin observed from the plot shows that the variation in the band gap can indeed be attributed to the Burstein Moss effect. The derived reduced effective mass correspond to ~0.84. This value is closer to values derived using heavy hole effective mass then the values obtained experimentally[38-39]. There is therefore a decrease in transparency in the UV region when the oxygen pressure is increased as the carrier concentration is lowered.

3.2 Effect of film thickness

The transparency and resistivity, as discussed in the previous section, show that multiple reasons can simultaneously account for the change in these two properties and, apart from those already mentioned, the effect of film thickness is not well understood. We investigated this effect by deposition of AZO films of different thickness on PET substrates at our optimum oxygen pressure at room temperature. The optimization was selected using a modified figure of merit (FOM) to better assess our deposited thin films. Haacke *et. al.* introduced a FOM (φ_{TC}) for transparent conductors defined as [40]

$$\varphi_{TC} = T^{10} / R_{sh} \tag{2}$$

where T is the transmittance at peak value and R_{sh} is the sheet resistance. A larger FOM therefore represents a better TCO. Using Eq. (2), the computed FOM of our deposited films used is shown in Table 1. However, the Haacke's FOM uses the peak value of transmission that may not be representative of the overall transmission. In this work, we use the normalized transparency index (TI) in a modified (FOM_{TI}) to give a more complete analysis. Not only does this normalization takes into account transparency across a suitable spectrum, this transparency is free of influence from any thickness variations. Our approach is more suitable if the FOM is to be used to compare across the variations in oxygen pressure since we want any changes in transparency to accurately reflect true changes in film properties. Using the modified FOM as a comparison, we concluded that an oxygen pressure of 1.3×10^{-2} Pa gives the best overall AZO properties in our setup.

At the optimum deposition condition, variations in film thickness show significant changes in the resistivity. The summary of the changes in electrical properties is shown in figure 6 and it is observed that thicker films generally give a lower resistivity and this is consistent with reports of AZO deposited on glass [41]. This improvement is often associated with improved film crystallinity. We therefore examined the XRD peaks of our deposited films as shown in figure 7(a). The XRD peaks show the dominant ZnO (002) peak for all thicknesses, with a difference in intensity due to the differences in thickness. The grain sizes as computed from the full width at half maximum of the observed peak increases slightly from 12.2 nm to 16.8 nm with film thicknesses. A plot of the variation in mobility with grain size is shown in figure 7(b). Unlike our previous observation at different oxygen pressures, the trend of

higher mobility for larger grain sizes can be observed for the case of different film thicknesses. Part of the reason may be that once the film growth is optimized in reducing defect related scattering, the effect of grain size can be more easily observed. On closer examination, it is noted that the larger improvements in mobility is observed when the films thickness is increased from <50 nm to 100 nm. At such small thicknesses, where grain sizes are comparable, film thickness may perhaps affect the growth of the grains. Therefore at larger film thicknesses, the increase of the grain size quickly saturates. The increase in film thickness showed substantial increase in carrier concentration and mobility (figure 6). If such variation of grain sizes is not responsible as was discussed, additional explanation is needed to account for the observations.

We believe that the improvements in the electrical properties of the films can be suitably explained by the influence from surface and interface effects. We note that the large increase in carrier concentration similarly affects the measured optical band gap as it is increased from ~3.38 to 3.75 eV as shown in a summary plot in figure 8. This is similarly a Burstein-Moss effect well demonstrated by the same increase of bandgap with the increase in carrier concentration. Since the films are deposited using the same condition, we expect little changes in the bulk film. We therefore attribute the changes to surface and near surface carrier depletion that is much more pronounced for thinner films. This depletion reduces the effective mobile carrier concentration and the resulting space charges that forms increases ionized impurity scattering and this can reduce the carrier mobility in the TCO. This hypothesis then describes well the observed saturation of both the increase in carrier concentration and mobility once larger film thicknesses are achieved, since bulk effects are likely to dominate.

The transparency of the films at different thicknesses is also compared after normalization as similarly shown in figure 8. The normalization ensures that we are primarily comparing film properties. Expectedly, there are not many changes in the transparency indices as observed since the films are grown under the same condition that reduces defect related absorption. The visible transparency shows comparable values while the decrease in the infrared transmittance is due to the decrease in mobile carriers as discussed above. From these observations, we can conclude that optical properties of the films in the visible range are not greatly affected by different thicknesses. Decreasing transparency is a direct result of thickness dependent absorption and not a reflection of true optical property changes.

Even though the above discussion highlighted that the inherent transparency does not vary significantly for the TCO, expected thickness dependent absorption still plays a role even for materials with low absorption coefficients or long attenuation lengths. Optimization of the TCO should therefore involve the optimization of the resistivity for the lowest possible film thickness. We summarize the obtained resistivity variations in this work and those that were reported in the literature as shown in figure 9. The general trend in variation of resistivity with film thickness agrees with the findings from this study. The optimum thickness of AZO must first satisfy its grain size restriction and for room temperature deposition, this is typically low. This means that suitable grain sizes can be achieved with thinner films of <100 nm. However, at such conditions, surface/interface depletion and scattering effects play an important role, meaning that the optimum thickness for thin films with small grain sizes are restricted

by a more general limit. Considering the thickness dependent attenuation, there should be an upper limit in terms of optimization of film thickness. Naturally, if annealing is involved and grain sizes are increased, this general limit will change. We also highlight that the obtained resistivity in this work shows excellent resistivity values for ZnO deposited on PET substrates and this is clearly depicted in figure 9. Unlike some of the data shown in the same plot, our highly conductive TCO is notably achieved at room temperature through the optimization of growth conditions, and this finding holds great promises for applications in flexible organic devices.

4. Conclusion

In summary, high-quality transparent conductive AZO thin films, deposited by pulsed laser deposition on low-cost flexible polyethylene terephthalate substrates, were investigated as a function of oxygen pressure and film thickness. Structural, electrical and optical properties of the AZO thin films were examined. We used a modified figure of merit to select the optimized deposition condition and investigate the effect of film thickness variations. It was found that grain sizes play only a greater role at smaller film thicknesses in affecting the carrier mobility for these room temperature deposited films. With increasing film thickness, near surface/interface depletion and scattering of carriers can affect the mobility and carrier concentration, thereby increasing the resistivity. This serves as a general limit for films with smaller grain sizes and is thus especially relevant for low temperature growth. Although transparency in the UV and infrared regions do change, these often compensate for each other and the visible transparency is not significantly affected. Considering finite attenuation effects of film thickness, this should serve as an upper limit for the thickness of TCOs in device

applications. In this work, we obtained a resistivity as low as ~6.6×10^{-4} Ω-cm with a high normalized transparency index of >0.78 (78% of total solar spectrum transmitted) for a 110 ± 10 nm thin film. This represents one of the best results obtained for such film thicknesses deposited at room temperature.

References

[1] K. Nomura, H. Ohta, A. Takagi, T. Kamiya, M. Hirano, H. Hosono, Nature 432 (2004) 488.

[2] E. Fortunato, P. Barquinha and R. Martins, Adv. Mater. 24 (2012) 2945.

[3] G. A. Niklasson, C. G. Granqvist, J. Mater. Chem. 17 (2007) 127.

[4] H. –C. Jau, K. –T. Cheng, T. –H. Lin, Y. –S. Lo, J. –Y. Chen, C. –W. Hsu, A. Y. –G. Fuh, Appl. Optics 50 (2011) 213.

[5] C. G. Granqvist, Sol. Energy Mater. Sol. Cells 91(2007) 1529.

[6] T. Minami, Semicond. Sci. Technol. 20 (2005) S35.

[7] N. R. Armstrong, P. Alex Veneman, .E. Ratcliff, D. Placencia, M. Brumbach, Acc. Chem. Res. 42 (2009) 1748.

[8] B. Yoo, K. Kim, S. H. Lee, W. M. Kim, N. –G. Park, Sol. Energy Mater. Sol. Cells 92 (2008) 873.

[9] D. S. Ginley, C. Bright, MRS Bull., 35 (2000) 15.

[10] N. Yamamoto, H. Makino, T. Yamada, Y. Hirashima, H. Iwaoka, T. Ito, A.Ujihara, H. Hokari, H. Morita, T. Yamamoto, J. Electrochem. Soc. 157 (2010) J13.

[11] R. Meerheim, R. Nitsche, K. Leo, Appl. Phys. Lett. 93 (2008) 043310.

[12] Y. B. Xiao, S. M. Kong, E. H. Kim, C. W. Chung, Sol. Energy Mater. Sol. Cells 95 (2011) 264.

[13] T. Hamaguchi, K. Omae, T. Takebayashi, Y. Kikuchi, N. Yoshioka, Y. Nishiwaki, A. Tanaka, M. Hirata, O. Taguchi, T. Chonan, Occup. Environ. Med. 65 (2008) 51.

[14] G. Khrypunov, A. Romeo, F. Kurdesau, D. L. Bätzner, H. Zogg, A. N. Tiwari, Sol. Energy Mater. Sol. Cells 90 (2006) 664.

[15] V. Bhosle, J. Narayan, J. Appl. Phys. 100 (2006) 093519.

[16] T. Minami, Thin Solid Films 516 (2008) 1314.

[17] K. Jung, W. –K. Choi, S. –J. Yoon, H. J. Kim, J. –W. Choi, Appl. Surf. Sci. 256 (2010) 6219.

[18] L. Gong, J. Lu, Z. Ye, Sol. Energy Mater. Sol. Cells 94 (2010) 937.

[19] E. Fortunato, L. Raniero, L. Silva, A. Gonçalves, A. Pimentel, P. Barquinha, H. Águas, L. Pereira, G. Gonçalves, I. Ferreira, E. Elangovan, R. Martins, Sol. Energy Mater. Sol. Cells 92 (2008) 1605.

[20] H. –K. Park, J –A. Jeong, Y. –S. Park, S. –I. Na, D. –Y. Kim, H. –K. Kim, Electrochem. Solid–State Lett. 12 (2009) H309.

[21] B. J. Lee, H. J. Kim, W. –I. Jeong, J. –J. Kim, Sol. Energy Mater. Sol. Cells 94 (2010) 542.

[22] K. Elmer, J. Phys. D: Appl. Phys. 34 (2001) 3097.

[23] J. E. Medvedeva, C. L. Hettiarachchi, Phys. Rev. B 81 (2010) 125116.

[24] H. J. Ko, Y.F. Chen, S.K. Hong, H. Wenisch, T. Yao, D.C. Look, Appl. Phys. Lett. 77 (2000) 3761.

[25] K. –I. Lee, E. K. Kim, H. –D. Kim, H. –I. Kang, J. –T. Song, Phys. Stat. Sol. (c) 5 (2008) 3344.

[26] L. Gong, J. Lu, Z. Ye, Sol. Energy Mater. Sol. Cells 94 (2010) 1282.

[27] X. –T. Hao, J. Ma, D. –H. Zhang, Y. –G. Yang, H. –L. Ma, C. –F. Cheng, X. –D. Liu, Mater. Sci. Eng. B 90 (2002) 50.

[28] A. Bowen, J. Li, J. Lewis, K. Sivaramakrishnan, T. L. Alford, S. Iyer, Thin Solid Films 519 (2011) 1809.

[29] E. Fortunato, P. Nunes, A. Marques, D. Costa, H. Águas, I. Ferreira, M. E. V. Costa, M. H. Godinho, P. L. Almeida, J. P. Borges, R. Martins, Surf. Coat. Technol. 151–152 (2002) 247.

[30] M. J. Gadre, T. L. Alford, Appl. Phys. Lett. 99 (2011) 051901.

[31] L. M. Wong, S. Y. Chiam , J. Q. Huang, S. J. Wang, W. K. Chim, J. S. Pan, Sol. Energy Mater. Sol. Cells 95 (2011) 2400.

[32] E. H. Kisi, M. M. Elcombe Acta Crystallogr., Sect. C: Cryst. Struct. Commun. 45 (1989) 1867 (ICDD ZnO pattern 00–036–1451).

[33] Q. –B. Ma, Z. –Z. Ye, H. –P. He, S. –H. Hu, J. –R. Wang, L. –P. Zhu, Y. –Z. Zhang, B. –H. Zhao, J. Cryst. Growth 304 (2007) 64.

[34] J. A. Sans, J. F. Sánchez-Royo, A. Segura, Superlattices Microstruct. 43 (2008) 362.

[35] E. Burstein, Phys. Rev. 93 (1954) 632.

[36] A. Segura, J. A. Sans, D. Errandonea, D. Martinez-García, V. Fages, Appl. Phys. Lett. 88 (2006) 011910.

[37] B. E. Sernelius, K. –F. Berggren, Z. –C. Jin, I. Hamburg, C. G. Granqvist, Phys. Rev. B, 37 (1988) 10244.

[38] S. L. Shi, S. J. Xu, J. Appl. Phys. 109 (2011) 053510.

[39] N. N. Syrbu, I. M. Tiginyanu, V. V. Zalamai, V. V. Ursaki, E. V. Rusu, Physica B 353 (2004) 111.

[40] G. Haacke, J. Appl. Phys. 47 (1976) 4086.

[41] B. –Z. Dong, G. –J. Fang, J. –F. Wang, W. –J. Guan, X. –Z. Zhao, J. Appl. Phys. 101 (2007) 033713.

[42] J. –M. Kim, P. Thiyagarajan, S. –W. Rhee, Thin Solid Films 518 (2010) 5860.

[43] J. –H. Lee, J. –T. Song, Thin Solid Films 516 (2008) 1377.

[44] J. Lee, D. Lee, D. Lim, K. Yang, Thin Solid Films 515 (2007) 6094.

[45] Y. S. Jung, H. W. Choi and K. H. Kim, S. J. Park, H. H. Yoon, J. Korean Phys. Soc. 55 (2009) 1945.

[46] X. T. Hao, J. Ma, D. H. Zhang, T. L. Yang, H. L. Ma, Y. G. Yang, C. F. Cheng, J. Huang, Appl. Surf. Sci. 183 (2001) 137.

[47] S. Fernández, F. B. Naranjo, Sol. Energy Mater. Sol. Cells 94 (2010) 157.

[48] J. –H. Lee, J. Electroceram. 23 (2009) 512.

Figure Captions

Figure 1 Normalized transparency index of AZO films at different indicated wavelength ranges as a function of oxygen pressure during deposition at room temperature. The corresponding measured resistivities of the films are also included.

Figure 2 (a) X-ray diffraction spectra of AZO thin films at various oxygen pressures deposited on PET substrates at room temperature. (b) Plot of spread in mobility for different measured grain sizes. The thin films were deposited at various oxygen pressures at room temperature.

Figure 3 Electrical resistivity (ρ), carrier concentration (n), and Hall mobility (μ) of the AZO films plotted as a function of oxygen pressure for deposition at room temperature.

Figure 4 Plot of $(\alpha E)^2$ as a function of photon energy for AZO films deposited at different oxygen pressures at room temperature.

Figure 5 Variation of the optical band gap plotted against the 2/3 power of carrier concentration ($n^{2/3}$). Dotted line shows the best fit data through the origin.

Figure 6 Electrical resistivity (ρ), carrier concentration (n), and Hall mobility (μ) of the AZO films as a function of film thickness for films deposited at an optimized oxygen pressure of 1.3×10^{-2} Pa at room temperature.

Figure 7 (a) X-ray diffraction spectra of AZO thin films at indicated thicknesses deposited on PET substrates at room temperature. (b) Plot of spread in mobility for different film thicknesses deposited at an optimized oxygen pressure.

Figure 8 Normalized (against thickness) transparency index at different wavelength ranges for films deposited at an oxygen pressure of 1.3×10^{-2} Pa at room temperature. Also included are the corresponding carrier concentration and optical band gap of the AZO films.

Figure 9 Variation in resistivity with film thickness obtained in this work. The values obtained from other independent reports of AZO on polymeric substrates are also shown. These values are obtained from reports as indicated by the reference number for each data point [25,27,29,40-46].

Table Captions

Table 1. Figure of merit and modified figure of merit for undoped ZnO and AZO samples at various oxygen pressure of similar thickness (indicated in Pa) and at same oxygen pressure of various thicknesses (indicated in nm).

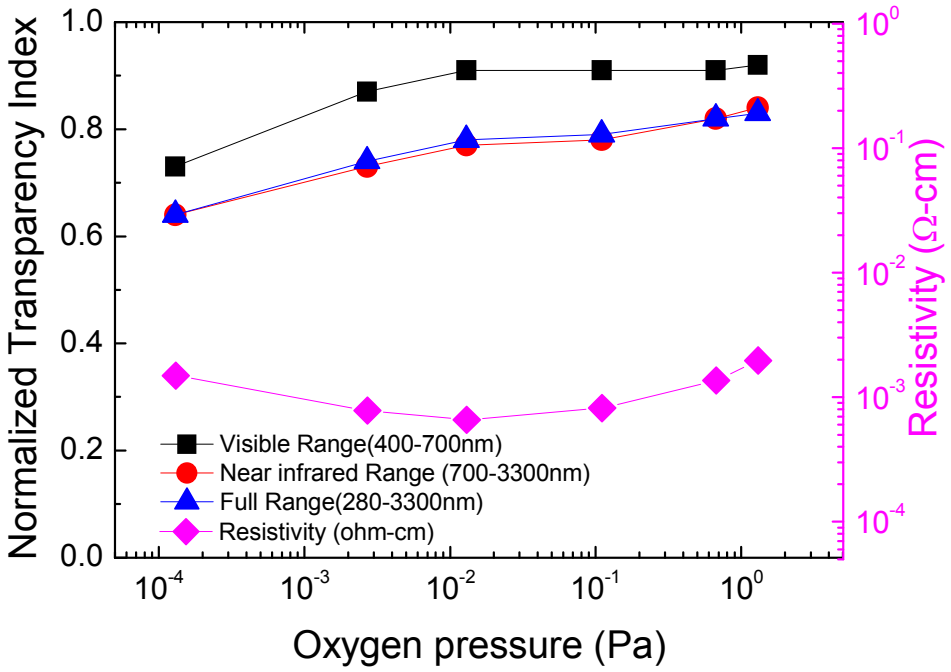

FIG. 1.
Wong *et al.*

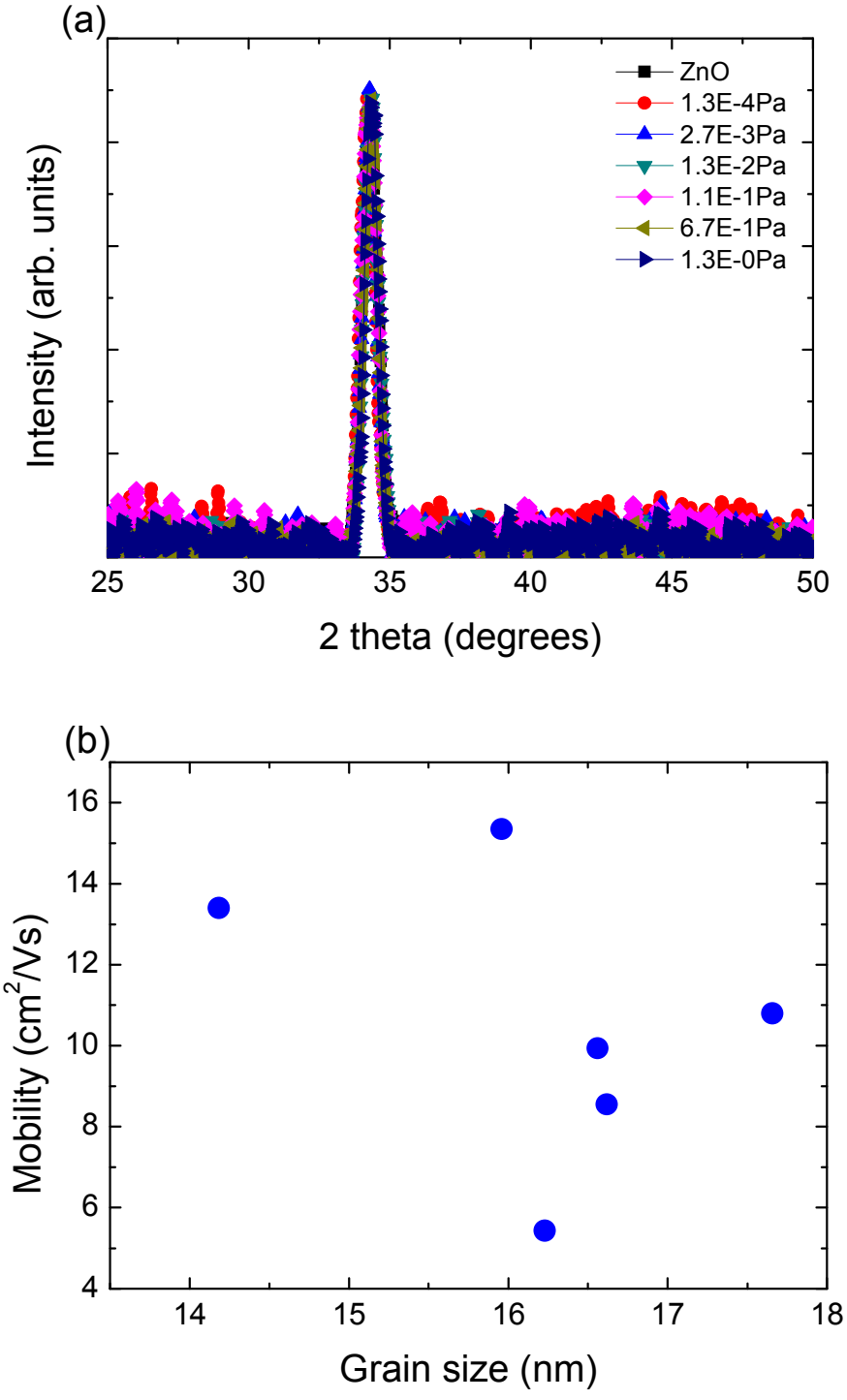

FIG. 2.
Wong *et al.*

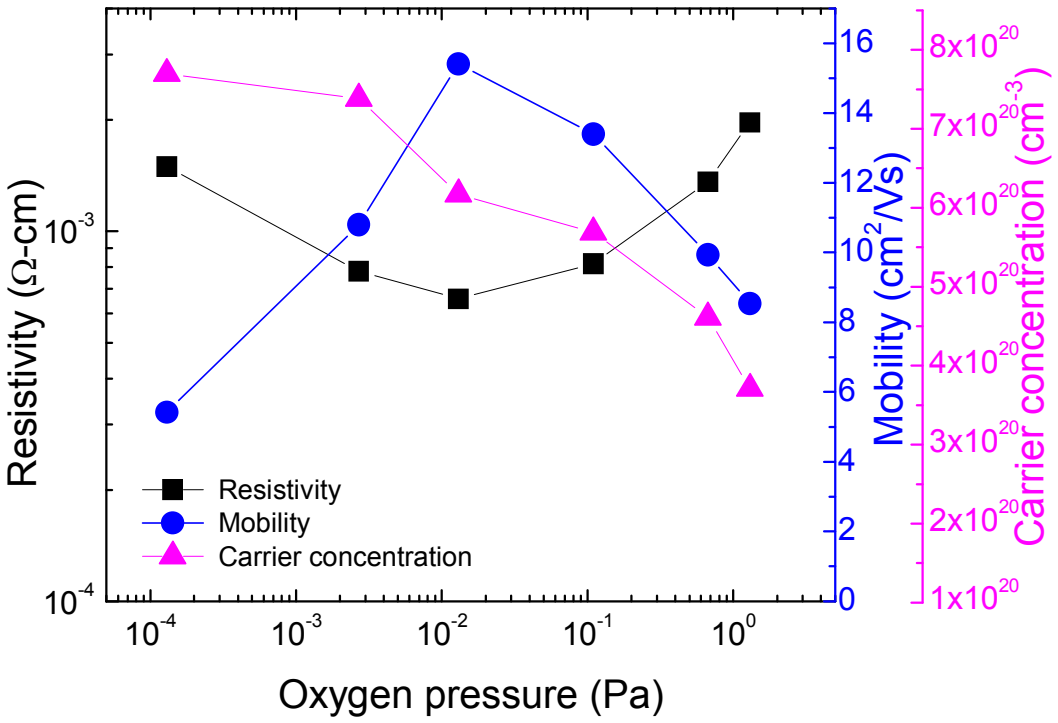

FIG. 3.
Wong *et al.*

Figure 4 is modified

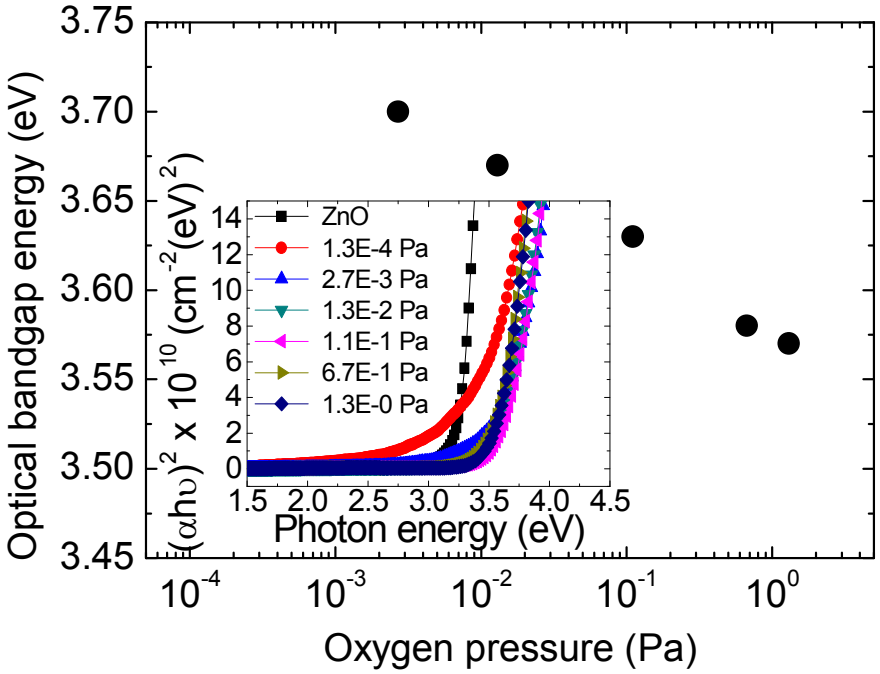

FIG. 4.
Wong *et al.*

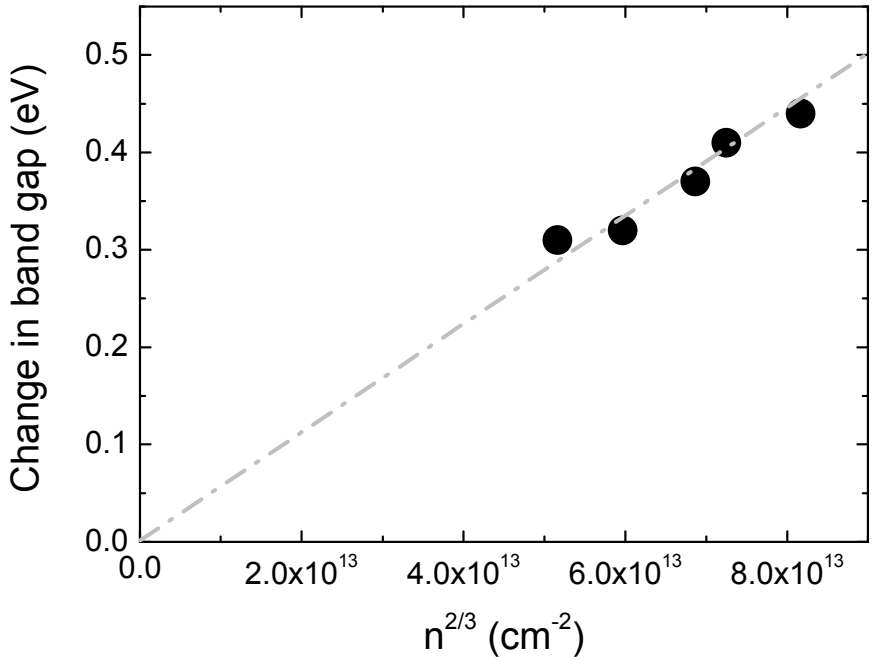

FIG. 5.
Wong *et al.*

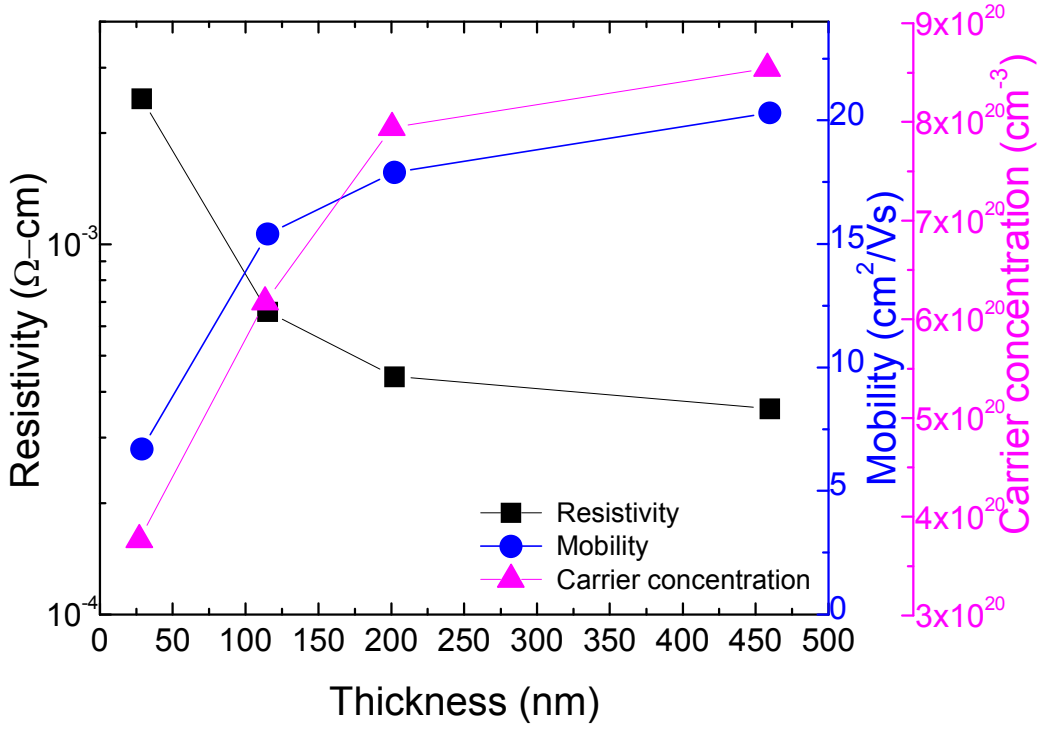

FIG. 6.
Wong *et al.*

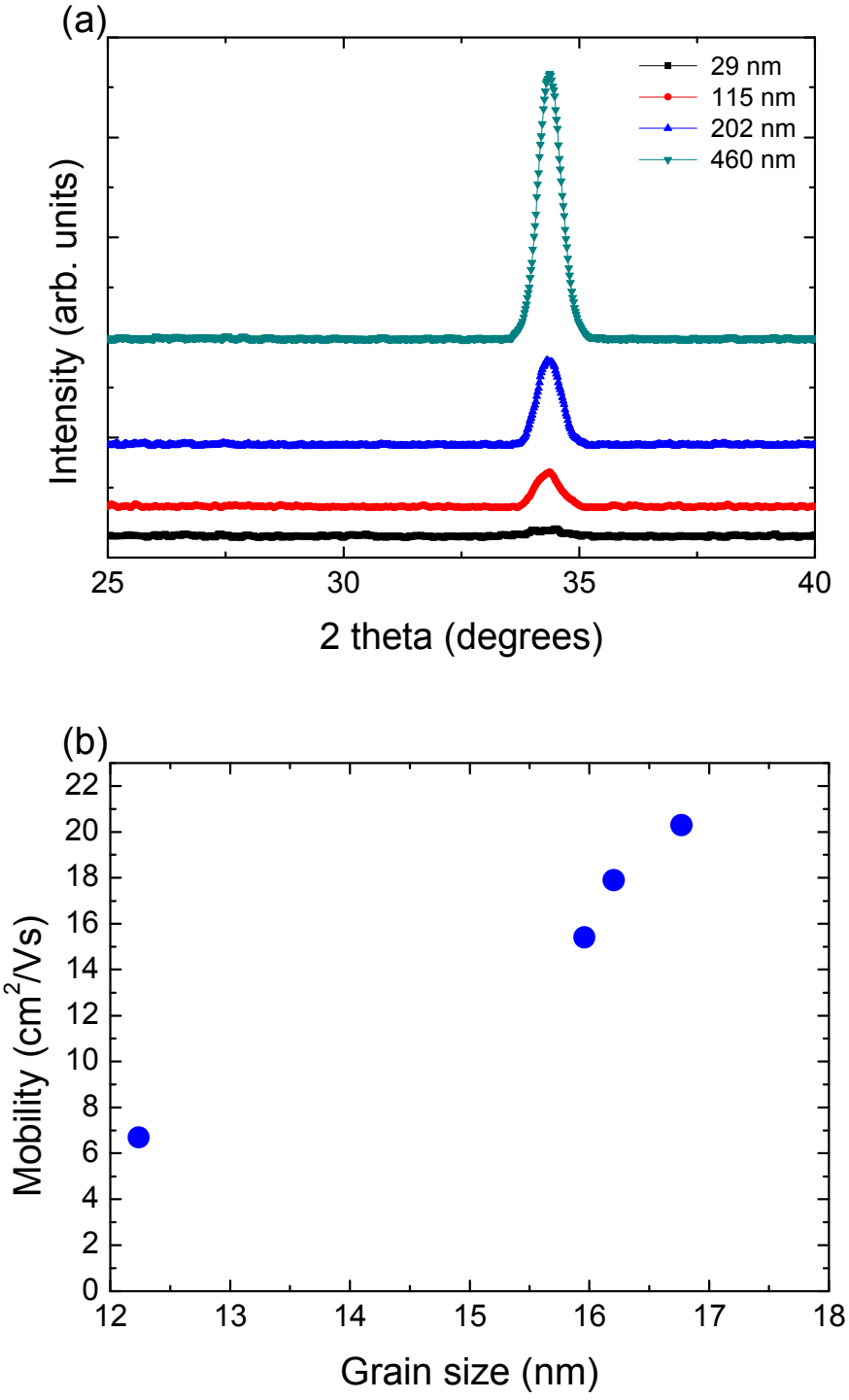

FIG. 7.
Wong *et al.*

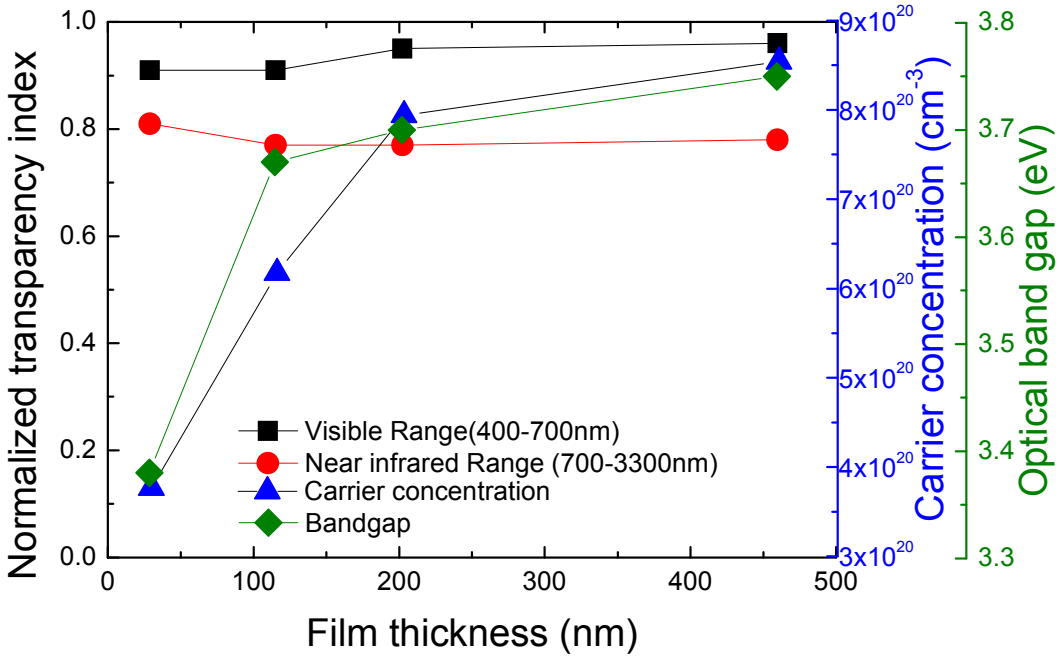

FIG. 8.
Wong *et al.*

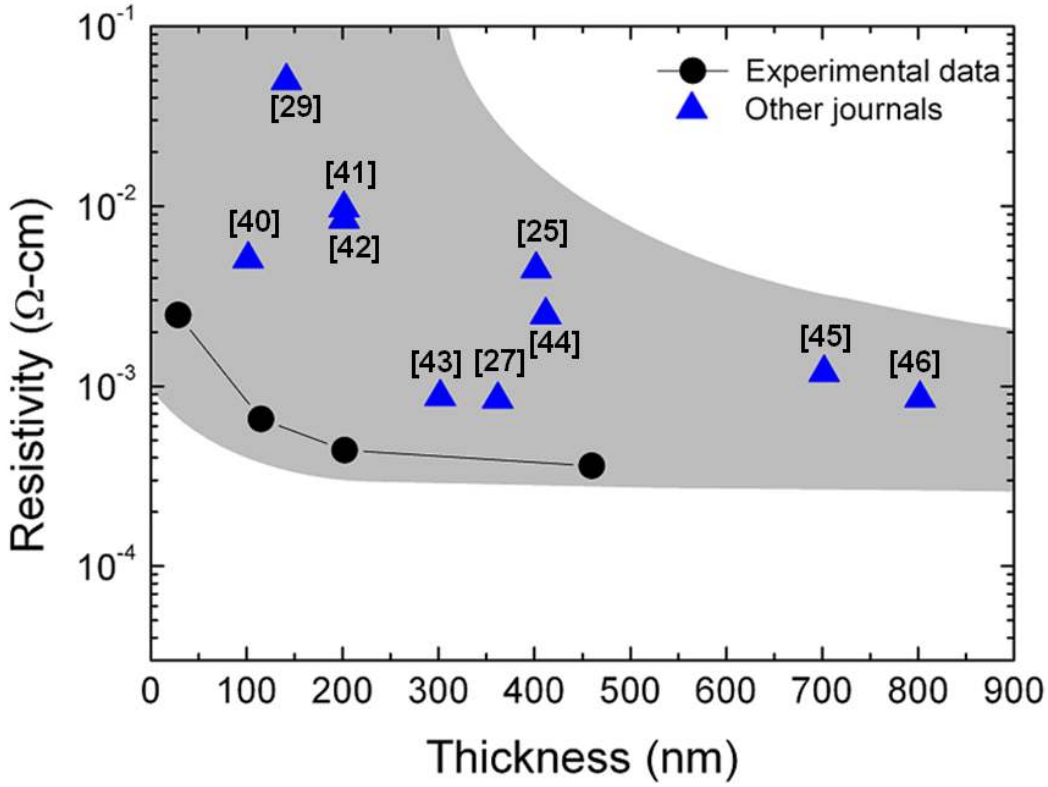

FIG. 9.
Wong *et al*

Sample	Haacke's Figure of merit, FOM (Ω^{-1})	Modified figure of merit, FOM_{TI} (Ω^{-1})
Undoped ZnO	2.77×10^{-3}	1.23×10^{-3}
1.3×10^{-4} Pa	4.63×10^{-4}	4.96×10^{-3}
2.7×10^{-3} Pa	5.34×10^{-3}	1.12×10^{-2}
1.3×10^{-2} Pa	9.51×10^{-3}	1.37×10^{-2}
1.1×10^{-1} Pa	7.09×10^{-3}	1.04×10^{-2}
6.7×10^{-1} Pa	4.62×10^{-3}	6.27×10^{-3}
1.3 Pa	3.37×10^{-3}	4.22×10^{-3}
29 nm	1.18×10^{-3}	9.30×10^{-4}
115 nm	9.51×10^{-3}	1.37×10^{-2}
202 nm	2.63×10^{-2}	3.65×10^{-2}
460 nm	3.66×10^{-2}	1.04×10^{-1}

Table 1
Wong *et al*